Pure Appl. Chem., Vol. 72, Nos. 1–2, pp. 37–45, 2000.

Synthesis of magnetic spinel ferrite $CoFe_2O_4$ nanoparticles from ferric salt and characterization of the size-dependent superparamagnetic properties*

Chao Liu, Adam J. Rondinone, and Z. John Zhang†

School of Chemistry and Biochemistry, Georgia Institute of Technology, Atlanta, Georgia 30332-0400, USA

Abstract: The $CoFe_2O_4$ nanoparticles have been synthesized by using a stable ferric salt of $FeCl_3$ with a micellar microemulsion method. The normal micelles are formed by sodium dodecyl sulfate (NaDS) in aqueous solutions. The mean size of the nanoparticles can be controlled from less than 4 nm to about 10 nm through controlling the concentrations of the reagents. The neutron diffraction in combination with the Rietveld refinement shows that these $CoFe_2O_4$ nanoparticles have a high degree of inversion with 66% of the tetrahedral sublattice occupied by Fe^{3+}. Magnetic measurements and neutron diffraction studies demonstrate the superparamagnetic nature of these $CoFe_2O_4$ nanoparticles. The size-dependent superparamagnetic properties of $CoFe_2O_4$ nanoparticles have also been systematically studied. The blocking temperature and coercive field of the nanoparticles increase with increasing size of the nanoparticles. The superparamagnetic behaviors of $CoFe_2O_4$ nanoparticles are consistent with the Stoner-Wohlfarth theory of single domain particles.

INTRODUCTION

Magnetic nanoparticles of spinel ferrites are of great interest in fundamental science, especially for addressing the fundamental relationships between magnetic properties and their crystal chemistry and structure. Superparamagnetism is a unique feature of magnetic nanoparticles and is crucially related to many modern technologies including ferrofluid technology [1], magnetocaloric refrigeration [2], contrast enhancement in magnetic resonance imaging (MRI) [3], and magnetically guided drug delivery [4]. Superparamagnetic properties have been extensively studied in the pure metal nanoparticles, such as Fe, Co, and Ni with the size confined within only a few nanometers [5–8], whose applications are limited by the poor chemical stability. Recently, more attention has been focused on the preparation and characterization of superparamagnetic metal oxide nanoparticles such as spinel ferrites, MFe_2O_4 (M = Co, Mg, Mn, Zn, etc.) [9–14]. The rich crystal chemistry in spinel ferrite systems offers excellent opportunities for understanding and fine-tuning the superparamagnetic properties of nanoparticles by chemical manipulations.

Spinel ferrite $CoFe_2O_4$ nanoparticles have been extensively studied. To date, $CoFe_2O_4$ nanoparticles are usually synthesized by co-precipitation or by microemulsion using normal micelles [15–17]. Microemulsion method has produced high-quality $CoFe_2O_4$ nanoparticles with a size distribution of about 15% or less. Since one of the starting reagents is chemically unstable ferrous salt, the synthesis process is complicated, and extra caution has to be exercised in order to obtain consistent products. We

Pure Appl. Chem.* **72, 1–331 (2000). An issue of reviews and research papers based on lectures presented at the 1st IUPAC Workshop on Advanced Materials (WAM1), Hong Kong, July 1999, on the theme of nanostructured systems.
†Corresponding author

herein report an experimental procedure for synthesizing $CoFe_2O_4$ nanoparticles from stable ferric salt. Magnetic measurements in combination with neutron diffraction studies demonstrate the superparamagnetic nature of these $CoFe_2O_4$ nanoparticles. The size-dependent superparamagnetic properties of $CoFe_2O_4$ nanoparticles have also been systematically studied. The blocking temperature and coercive field of the nanoparticles clearly show size dependence. The superparamagnetic behaviors of $CoFe_2O_4$ nanoparticles are consistent with the Stoner–Wohlfarth theory of single domain particles.

EXPERIMENTAL

Nanoparticle synthesis

$CoFe_2O_4$ nanoparticles have been synthesized by microemulsion method through the formation of normal micelles using sodium dodecyl sulfate (NaDS) (Aldrich, 98% pure) as surfactant. The reagents $CoCl_2 \cdot 6H_2O$ (Fisher, 98.7% pure) and $FeCl_3 \cdot 6H_2O$ (Aldrich, 98.0% pure) were mixed in an aqueous solution with the ratio of Co to Fe as 1:2. An aqueous solution of surfactant was added to form a mixed micellar solution of $Co(DS)_2$ and $Fe(DS)_3$. After aqueous methylamine (Aldrich, 40 wt. % in water) solution was added into the mixture above 50 °C, a dark slurry was formed. Then the reaction mixture was stirred vigorously for 3 h above 50°C. After the $CoFe_2O_4$ nanoparticles were isolated by centrifugation, the nanoparticles were washed with water and ethanol to remove the excess surfactant. $CoFe_2O_4$ nanoparticulate powder was obtained after the sample was dried overnight in a vacuum oven at 100 °C. The size of $CoFe_2O_4$ nanoparticles is controlled by the experimental conditions such as the concentration of Co^{2+} and Fe^{3+} salts and the amount of methylamine added.

X-ray diffraction

X-ray diffraction data were collected with a Bruker D8 ADVANCE X-ray diffractometer. Kα radiation from a Cu target has been employed. The peak broadening data are obtained by measuring the average of peak broadening in the five strongest diffraction peaks.

Neutron diffraction

Neutron diffraction studies have been conducted by using the HB4 powder diffractometer at the High-Flux Isotope Reactor (HFIR) of Oak Ridge National Laboratory. The $CoFe_2O_4$ nanoparticles were placed in vanadium cans in a vacuum furnace. The heating element for diffraction at 100 °C was a niobium rod. The data collection was over the 2-theta range of 11° to 135° in steps of 0.05°. The sample temperature in the furnace was calibrated using the thermal expansion of magnesium oxide. The wavelength was precisely determined to be 1.4997(1) Å based upon the refinements of Si standard. The diffraction data were corrected for the variation in detector efficiencies, which were determined by using a vanadium standard.

Characterization of magnetic properties

Magnetic measurements of $CoFe_2O_4$ nanoparticles were carried out with a Quantum Design MPMS-5s superconducting quantum interference device (SQUID) magnetometer. The maximum strength of the magnetic field is 5 T. In the hysteresis measurements at low temperature, the $CoFe_2O_4$ nanoparticles were mixed with eicosane ($C_{20}H_{42}$), which is a long-chain hydrocarbon compound with a melting point of 36.8 ºC. Eicosane formed a solid matrix to prevent these nanoparticles physically shifting positions.

RESULTS AND DISCUSSION

X-ray diffraction studies identify that these nanoparticulate samples are of pure $CoFe_2O_4$ spinel phase (Fig. 1). The mean size of the nanoparticles is determined from the peak broadening in the X-ray diffraction pattern by using the Debye–Scherrer equation. Transmission electron microscopy studies show that the size distribution in these $CoFe_2O_4$ nanoparticles is around 15% or less. Elemental analysis by inductively coupled plasma (ICP) method confirms that the ratio of Co to Fe is 1:2.

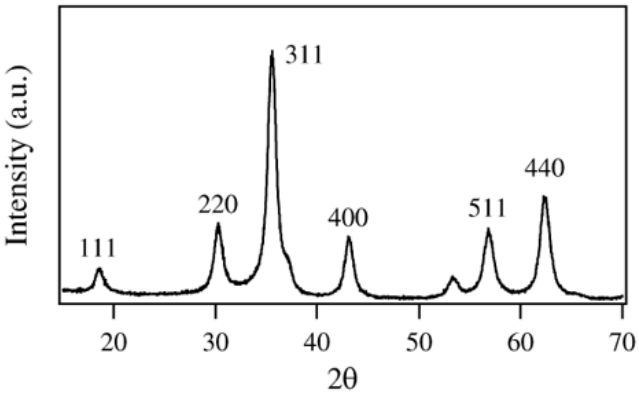

Fig. 1 X-ray diffraction pattern (Cu K_α-radiation) of $CoFe_2O_4$ nanoparticles with a mean diameter of 9.6 nm.

Neutron diffraction studies have been performed at 373 K to determine the magnetic state in these $CoFe_2O_4$ nanoparticles. The Rietveld refinement of the neutron diffraction pattern using the GSAS program shows an antiferromagnetic order in these nanoparticles (Fig. 2). This is certainly consistent with the ferrimagnetic nature of spinel ferrites [18]. The unambiguous magnetic order at 373 K in $CoFe_2O_4$ nanoparticles is no surprise since $CoFe_2O_4$ spinel ferrites have a Curie temperature as high as 790 K. The information on the cation distribution in these nanoparticles has also been extracted from

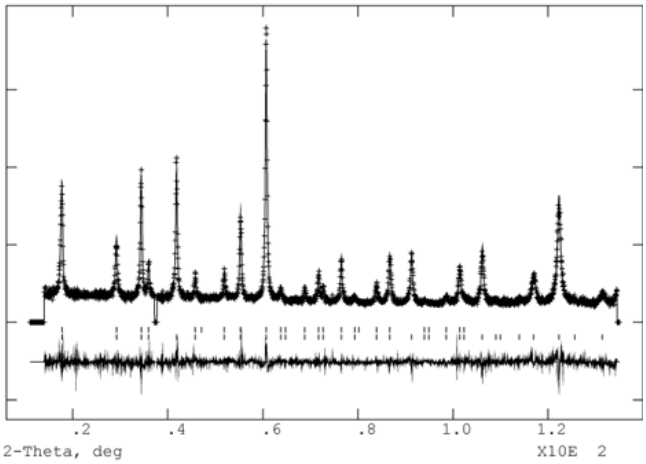

Fig. 2 Neutron diffraction patterns of 9.6 nm $CoFe_2O_4$ nanoparticles at 373 K. The "goodness of fit", χ^2 is 1.15. Below the pattern, the first row of the sticks marks the peaks from the magnetic scattering of $CoFe_2O_4$ nanoparticles. And the second row of the sticks corresponds to the peaks from the nuclear scattering. The excluded region near $2\theta = 38°$ eliminates the 110 diffraction peak of the Nb heating element of the furnace.

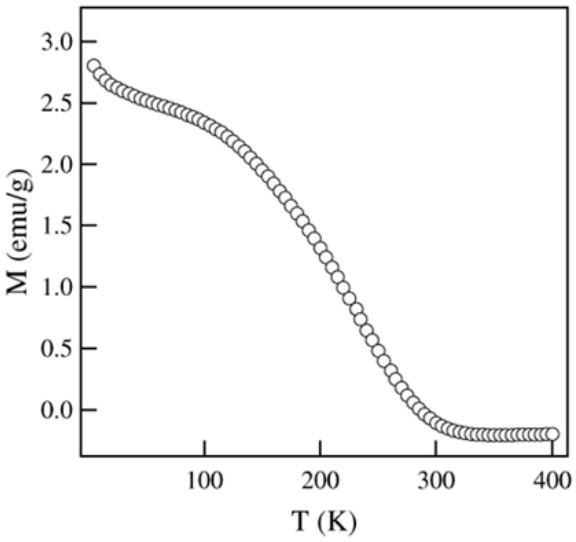

Fig. 3 Thermal decay of magnetization from 8.5-nm $CoFe_2O_4$ nanoparticles that have been cooled under a magnetic field of 100 G.

the Rietveld refinement of the neutron diffraction pattern. These $CoFe_2O_4$ nanoparticles have a cation occupancy inversion of 66% with a formula of $(Co_{0.34}Fe_{0.66})[Co_{0.32}Fe_{0.68}]O_4$ where cations in parenthesis and square bracket represent the occupancies at tetrahedral and octahedral sites, respectively. The unit cell is cubic and has a lattice constant of 8.388(7) Å. The magnetic moment is $3.58\mu_B$ at the tetrahedral lattice site and $-2.15\mu_B$ at the octahedral site.

The thermal remanent measurement has been conducted on these $CoFe_2O_4$ nanoparticles. The nanoparticulate sample is cooled to 5 K under a 100 G magnetic field. After the field is turned off, the temperature-dependent magnetization is measured as temperature rises from 5 K. Figure 3 shows a typical decay of the thermal remanent magnetization of these nanoparticles. The remanent magnetization of the $CoFe_2O_4$ nanoparticles having a mean diameter of 8.5 nm decreases rapidly with increasing temperature. When temperature increases to 290 K, the remanent magnetization of these nanoparticles is completely lost, and the nanoparticles become demagnetized.

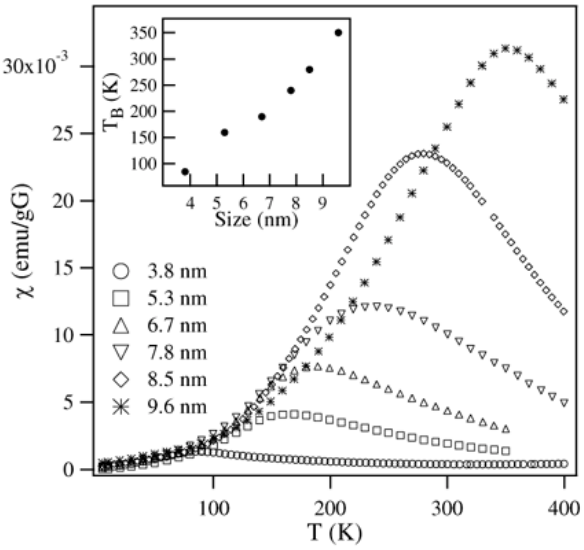

Fig. 4 Magnetic susceptibility vs. temperature for $CoFe_2O_4$ nanoparticles with various sizes. The applied field is 100 G. The inset shows the correlation between the blocking temperature and the mean particle size.

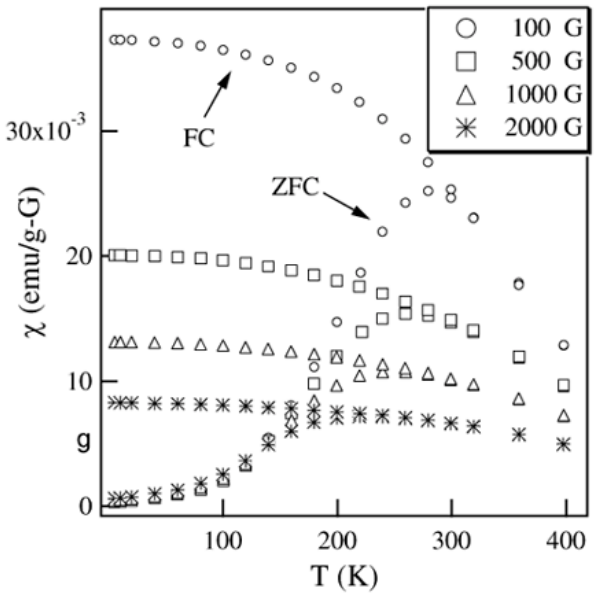

Fig. 5 Temperature dependence of magnetic susceptibility for zero-field-cooled (ZFC) and field-cooled (FC) 8.5-nm $CoFe_2O_4$ nanoparticles under various magnetic fields.

The magnetic susceptibility measurements of $CoFe_2O_4$ nanoparticles clearly show their dependence on the temperature and the nanoparticle size. In a typical measurement, the nanoparticulate sample is cooled from room temperature to 5 K without any external magnetic field applied. Then, a magnetic field of 100 G is applied, and the magnetization is recorded as the temperature slowly rises. The magnetic susceptibility of $CoFe_2O_4$ nanoparticles measured from 5 K to 350–400 K is shown as a function of temperature in Fig. 4. The magnetic susceptibility initially increases and eventually reaches a maximum at a certain temperature. The temperature, at which the maximum susceptibility is achieved, is the blocking temperature, T_B of the nanoparticulate sample and will be discussed in detail later. The blocking temperature of the nanoparticles clearly correlates with the size of the nanoparticles and increases as the mean diameter of the nanoparticles increases (inset in Fig. 4).

The temperature-dependent susceptibility of the $CoFe_2O_4$ nanoparticles also shows a divergence with different initial cooling processes. Figure 5 shows the susceptibility of the nanoparticles with a mean diameter of 8.5-nm cooled with a field cooling (FC) process or a zero field cooling (ZFC) process. When the nanoparticles are cooled and also measured under a 100 G field, the highest susceptibility is at 5 K, and it decreases steadily with increasing temperature. When the same nanoparticulate sample is cooled with the ZFC process, the susceptibility measured under a 100 G field shows an initial increase. When temperature reaches the blocking temperature of about 280 K, the magnetic susceptibility starts decreasing (top set of plots in Fig. 5). Also, this curve overlaps with the one obtained from the FC process at temperature above 280 K. The blocking temperature of the same nanoparticles decreases with increasing magnetic field strength. When the applied field in FC processes and in the subsequent magnetic susceptibility measurements increases to 500 G, 1000 G, and 2000 G, T_B of these 8.5-nm $CoFe_2O_4$ nanoparticles decreases to 260 K, 235K, and 215 K, respectively (Fig. 5).

The field-dependent magnetization of the $CoFe_2O_4$ nanoparticles clearly displays hysteresis below the blocking temperature. Figure 6 shows the hysteresis loops of the $CoFe_2O_4$ nanoparticles with different mean particle sizes at 5 K. The coercivity of the nanoparticles increases with increasing particle size as shown in Fig. 7. The saturation magnetization of the $CoFe_2O_4$ nanoparticles also increases with increasing particle size. Figure 8 shows the size dependence of the saturation magnetization, which is obtained by extrapolating M vs. 1/H plot to 1/H = 0. The coercivity of the nanoparticles decreases as

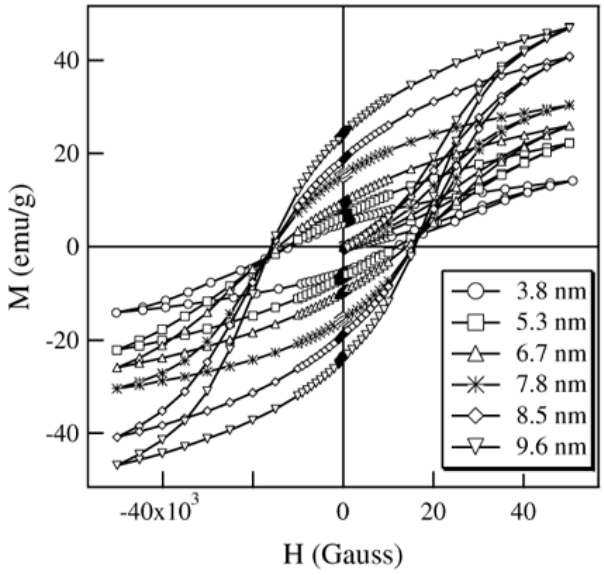

Fig. 6 Hysteresis of $CoFe_2O_4$ nanoparticles with various sizes at 5 K.

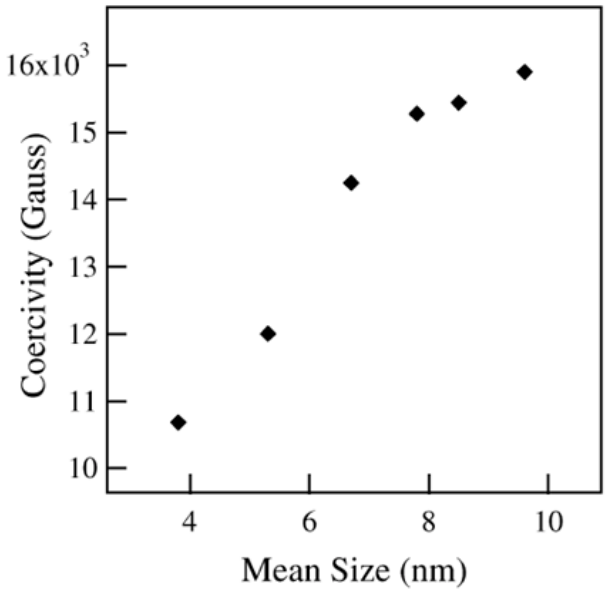

Fig. 7 The correlation between the coercivity and the mean nanoparticle size.

temperature increases. Figure 9 displays the hysteresis loops of the $CoFe_2O_4$ nanoparticles with a mean size of 6.7 nm at different temperatures. Although the coercivity of the nanoparticles rapidly decreases with increasing temperature, the maximum magnetization in a 5 T field remains almost unchanged. As the temperature approaches the blocking temperature of the 6.7-nm nanoparticles at 200 K, the coercivity reduces to zero (inset in Fig. 9). As the hysteresis vanishes at 200 K, the magnetization direction of the nanoparticles simply follows the direction of the applied magnetic field without any hysteretic hindrance.

The thermal remanent measurement shows that the magnetization of 6.7-nm $CoFe_2O_4$ nanoparticles vanishes above 200 K (Fig. 3). Consistently, the susceptibility of these nanoparticles displays paramag-

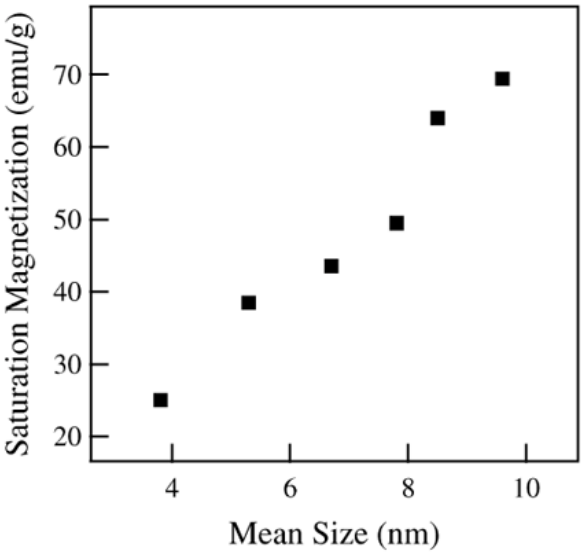

Fig. 8 The correlation between the saturation magnetization and the mean nanoparticle size.

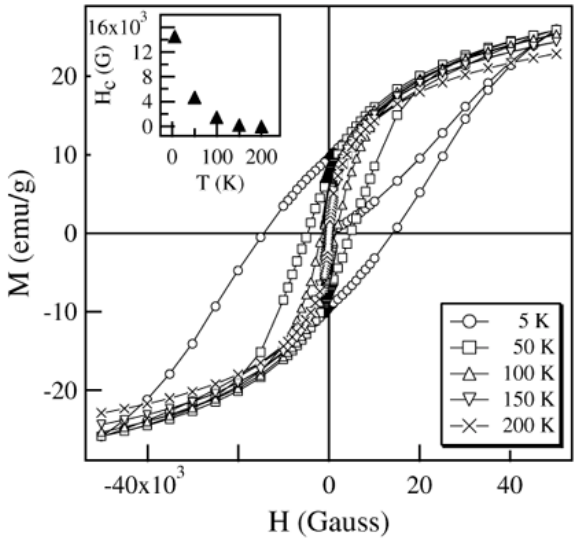

Fig. 9 Hysteresis of 6.7-nm $CoFe_2O_4$ nanoparticles at various temperatures. The inset displays the correlation between the coercivity, H_C of the nanoparticles and the temperature.

netic features at such a temperature range as Fig. 4 shows. For the $CoFe_2O_4$ nanoparticles with other mean diameters, they also show paramagnetic properties above the blocking temperature. Although the $CoFe_2O_4$ nanoparticles with a mean particle diameter of 9.6 nm have paramagnetic characteristics above 360 K (Fig. 4), the neutron diffraction studies on these nanoparticles display a well-defined magnetic order in each nanoparticle at 373 K (Fig. 2). These results unambiguously demonstrate that these $CoFe_2O_4$ nanoparticles are typical superparamagnetic nanoparticles. All the magnetic properties of these $CoFe_2O_4$ nanoparticles are consistent with the characteristics of a superparamagnetic system. In the superparamagnetic state, each nanoparticle behaves like a paramagnetic atom with the magnetization direction of each nanoparticle flipping randomly although the magnetic order still exists in each of the nanoparticles.

The correlation between the superparamagnetic properties of $CoFe_2O_4$ nanoparticles and the nanoparticle size is consistent with the size dependence of the magnetic anisotropy in the nanoparticles.

According to the Stoner–Wohlfarth theory, the magnetic anisotropy E_A of a single domain particle can be expressed as:

$$E_A = KV\sin^2\theta \quad (1)$$

where K is the magnetocrystalline anisotropy constant, V is the volume of the nanoparticle, and θ is the angle between the magnetization direction and the easy axis of the nanoparticle. This anisotropy serves as the energy barrier to prevent the change of magnetization direction [19]. When the size of magnetic nanoparticles is reduced to a threshold value, E_A is comparable with thermal activation energy, k_BT with k_B as the Boltzman constant, the magnetization direction of the nanoparticle can be easily moved away from the easy axis by thermal activation and/or an external magnetic field.

In thermal remanent measurements, the magnetization direction of the nanoparticles is frozen to the direction of applied magnetic field when the nanoparticles are cooled from room temperature to 5 K under a magnetic field. Even when the applied field is turned off, the anisotropy barrier prevents the magnetization direction of each nanoparticle from flipping. Therefore, a maximum magnetization is recorded at 5 K in Fig. 3. The magnetic anisotropy is not uniform in the randomly arranged nanoparticulate samples. A distribution of anisotropy energy exists [17]. As temperature rises, thermal activation energy starts to overcome the anisotropy energy barrier in some nanoparticles and frees the orientation of the magnetization direction in these nanoparticles. Due to the random flipping of the magnetization direction, the nanoparticles with their anisotropy barriers overcome give a time-averaged zero magnetization. Consequently, the remanent magnetization decreases with increasing temperature (Fig. 3). At the blocking temperature, almost every nanoparticle has its anisotropy overcome, and the total magnetization of the nanoparticles approaches zero.

The blocking temperature is the threshold point of thermal activation for the whole nanoparticulate sample. When the nanoparticles are cooled without a magnetic field, the magnetization direction of each nanoparticle aligns with its easy axis as temperature decreases below the blocking temperature. Due to the random orientation of the easy axes among the nanoparticles, overall susceptibility is almost zero since the applied field for susceptibility measurement is too small to overcome the anisotropy alone (Fig. 4). Above T_B, magnetic anisotropy is overcome by thermal activation, and the magnetization direction of each nanoparticle simply follows the applied field direction. Consequently, the nanoparticles become superparamagnetic and show paramagnetic properties. The larger the particles, the higher the E_A, the larger k_BT is required to become superparamagnetic. Therefore, T_B increases with increasing particle size.

The divergence between the susceptibility in a ZFC process and in a FC process is a characteristic feature of superparamagnetic behavior (Fig. 5). Such a divergence originates from the anisotropy barrier blocking of the magnetization orientation in the nanoparticles cooled with a ZFC process [17]. When a stronger magnetic field is applied, the magnetization direction of the nanoparticles becomes easier to switch to the field direction, and less assistance is required from the thermal activation. Consequently, the blocking temperature shifts to a lower value with a larger applied field (Fig. 5).

The coercivity of the nanoparticles is closely related to the magnetic anisotropy. At a constant temperature below T_B, the coercivity corresponds to the magnetic field strength at which the magnetic field provides the required energy in addition to the thermal activation energy to overcome the magnetic anisotropy. Therefore, the coercivity of the nanoparticles increases with increasing nanoparticle size (Figs. 6 and 7). As temperature increases, the required field strength for overcoming the anisotropy decreases (Fig. 9). When the temperature reaches the blocking temperature, thermal activation alone can overcome the magnetic anisotropy, and the coercivity reduces to zero (inset in Fig. 9). Certainly, the superparamagnetic nanoparticles do not display any magnetization hysteresis above the blocking temperature.

CONCLUSIONS

$CoFe_2O_4$ nanoparticles have been synthesized from a ferric salt. With the reagent as stable as ferric salt, the synthesis of $CoFe_2O_4$ nanoparticles is much easier to carry out. These $CoFe_2O_4$ nanoparticles have typical superparamagnetic properties. Neutron diffraction studies at an elevated temperature have confirmed the superparamagnetic nature of these nanoparticles. Their superparamagnetic behavior, such as the blocking temperature and coercivity, unambiguously correlates with the particle size. Such correlation is consistent with the Stoner–Wohlfarth theory on single domain particles.

ACKNOWLEDGMENTS

We thank Dr. Bryan Chakoumakos of Oak Ridge National Laboratory for his help in neutron diffraction studies. A. J. R. is partially supported by a Cherry Henry Emerson Chemistry Fellowship. We gratefully acknowledge the financial support in part from NSF (DMR-9875892) and the Beckman Young Investigator program of the Arnold and Mabel Beckman Foundation. The neutron diffraction studies have been carried out at Oak Ridge National Laboratory, which is managed by Lockheed Martin Energy Research Corp. for the U.S. Department of Energy under contract number DE-AC0596OR22464.

REFERENCES

1. K. Raj, R. Moskowitz, R. Casciari. *J. Magn. Magn. Mater*. **149**, 174 (1995).
2. R. D. McMichael, R. D. Shull, L. J. Swartzendruber, L. H. Bennett. *J. Magn. Magn. Mater*. **111**, 29 (1992).
3. D. G. Mitchell. *J. Magn. Reson. Imaging* **7**, 1 (1997).
4. U. Häfeli, W. Schütt, J. Teller, M. Zborowski, eds. *Scientific and Clinical Applications of Magnetic Carriers*, Plenum, New York (1997).
5. S. Yatsuya, T. Hayashi, H. Akoh, E. Nakamura, T. Akira. *Japan J. Appl. Phys*. **17**, 355 (1978).
6. R. B. Goldfarb and C. E. Patton. *Phys. Rev. B* **24**, 1360 (1981).
7. S. K. Khanna and S. Linderoth. *Phys. Rev. Lett*. **67**, 742 1991.
8. J. P. Chen, C. M. Sorensen, K. J. Klabunde, G. C. Hadjipanayis. *J. Appl. Phys*. **76**, 6316 (1994).
9. J. A. L. Perez, M. A. L. Quintela, J. Mira, J. Rivas, S. W. Charles. *J. Phys. Chem. B* **101**, 8045 (1997).
10. Q. Chen and Z. J. Zhang. *Appl. Phys. Lett*. **73**, 3156 (1998).
11. Z. X. Tang, C. M. Sorensen, K. J. Klabunde, G. C. Hadjipanayis. *J. Colloid Interface Sci.* **146**, 38 (1991).
12. C. T. Seip, E. E. Carpenter, C. J. O'Connor, V. T. John, S. Li. *IEEE Tans. Magn*. **34**, 1111 (1998).
13. J. F. Hochepied, P. Bonville, M. P. Pileni. *J. Phys. Chem. B* **104**, 905 (2000).
14. C. Liu, B. Zou, A. J. Rondinone, Z. J. Zhang. *J. Phys. Chem. B* **104**, 1141 (2000).
15. N. Moumen and M. P. Pileni. *Chem. Mater*. **8**, 1128 (1996).
16. M. P. Pileni and N. Moumen. *J. Phys. Chem*. **100**, 1867 (1996).
17. A. J. Rondinone, A. C. S. Samia, Z. J. Zhang. *J. Phys. Chem. B* **103**, 6876 (1999).
18. V. A. M. Brabers. In *Handbook of Magnetic Materials*, Vol. 8, K. H. J. Buschow, ed., p. 189, North-Holland, Amsterdam (1995).
19. E. C. Stoner and E. P. Wohlfarth. *Phil. Trans. Roy. Soc. A* **240**, 599 (1948), reprinted in *IEEE Trans. Magn*. **27**, 3475 (1991).